



# Development of composite silver/nickel nanopastes for low temperature joining of yttria-stabilized zirconia to stainless steels

A.H. Gorji<sup>a</sup>, A. Simchi<sup>a,b,\*</sup>, A.H. Kokabi<sup>a</sup>

<sup>a</sup>Department of Materials Science and Engineering, Sharif University of Technology, PO Box 11365-9466, 14588 Tehran, Iran

<sup>b</sup>Institute for Nanoscience and Nanotechnology (INST), Sharif University of Technology, 14588 Tehran, Iran

Received 23 August 2014; received in revised form 25 September 2014; accepted 26 September 2014

Available online 6 October 2014

## Abstract

Joining of yttria-stabilized zirconia (YSZ) to stainless steels is considered for various applications such as solid oxide fuel cells, thermal barrier coatings, and medical implants. In the present work, a series of brazing pastes utilizing silver and nickel nanoparticles ( $\sim 80$  nm) mixed with carboxymethyl cellulose as the organic phase were developed to join 5 mol% YSZ to AISI 420 steel. Effects of processing parameters including time and temperature of brazing and the composition of the nanopastes on the microstructure of joints and their shear rupture strength were studied. Elaboration of the joining mechanism by scanning electron microscopy and electron probe micro-analyzer showed solid-state sintering of the nanoparticles. Limited diffusion of the elements in the 420 SS part caused interface formation with a spongy structure. Increasing of the paste solid loading increased the density of the spongy structure at the interface region; thereby higher mechanical strength was attained. The joining was more successful when a silver nanopaste was utilized owing to the higher sintering activity of silver nanoparticles compared to nickel at relatively low brazing temperatures. Meanwhile, at high solid loadings, localized nanoparticle aggregation and microstructural heterogeneity at the interface region were observed. Increasing of the brazing time and temperature enhanced the diffusion of elements and improved the joint strength. Optimization of the processing parameters by the L16 Taguchi method determined that a silver paste with 72% solid loading processed at 270 °C for 120 min would yield a sound joint with shear strength of  $23 \pm 1$  MPa.

© 2014 Elsevier Ltd and Techna Group S.r.l. All rights reserved.

**Keywords:** C. Strength; Lead-free nanopaste; Low-temperature brazing; Nanoparticles; Silver; Yttria-stabilized zirconia

## 1. Introduction

Advanced ceramics with outstanding properties such as high corrosion and wear resistance, low density and suitable mechanical stability at elevated temperatures have wide applications in electronic devices, hip and bone transplants, and structural applications such as heat engines, turbines and automotive components [1]. To adapt the properties to a desired application, ceramic-metal joints have been developed. Examples of such applications include solid oxide fuel cells [2], circuit boards [3], nuclear instruments [4], hip replacement [5], and turbine blade

[6]. These functional materials provide an excellent combination of properties of both metals and ceramics in an integrated part. Therefore, in recent years joining of ceramics to metals have attracted significant attention [7]. Due to differences in the nature of atomic bonding, melting temperature and thermo-mechanical properties of ceramics and metals, preparation of sound and defect-free joints with a high mechanical stability is challenging. So far, various methods such as brazing [8], soldering [9], co-sintering [10], spark-plasma sintering [11] and sputtering [12] have been developed and utilized. Each of these processes has some advantages and disadvantages that make them suitable for specific applications.

One of the most interesting ceramic-metal joints with wide industrial applications is stabilized zirconia–stainless steel connections [13]. Zirconia with high flexural strength ( $\sim 1$  GPa), reasonable toughness ( $\sim 10$  MPa m<sup>0.5</sup>), and proper stability

\*Corresponding author at: Department of Materials Science and Engineering, Sharif University of Technology, PO Box 11365-9466, 14588 Tehran, Iran. Tel.: +98 (21) 6616 5261; fax: +98 (21) 66005717.

E-mail address: [simchi@sharif.edu](mailto:simchi@sharif.edu) (A. Simchi).

and electrical conductivity at elevated temperatures is a promising candidate to be used as anode in solid oxide fuel cells (SOFC) [14], thermal barrier coating (TBC) in aerospace shuttles [15–17], hip replacement in bone fracture [5], crowns in dental treatments [18], and protecting coatings in boiling water reactors [19]. On the other hand, stainless steels are fairly cheap while having high mechanical strength and ductility with good thermal-shock resistivity [20]. To prepare YSZ–SS joints, electron-beam evaporation [21], magnetron sputtering [22], electrophoresis [23], sol–gel [24], electrochemical deposition [25], superplastic joining [26], co-sintering [10] and active metal brazing [27] have been utilized. The latter is a promising approach because it is a facile method with low-processing cost, which does not require specific and high investment equipments [28]. In this technique, foils of active metals such as Ti and Ni were inserted between the ceramic and metal parts and brazed. Melting of the active layer occurs at the brazing temperature, results in wetting of the surfaces and causes interface formation. However, relatively high temperatures have to be utilized to melt the active layer which during cooling may induce cracks or deflection [29]. Particle-loaded pastes can be utilized to overcome these barriers [30]. Recently, Herring [31] has shown that micron-sized silver particles could be used for low-temperature joining. He has inserted a thin layer of silver paste between the joining couples and employed pressure-assisted sintering to form a joint. Albeit the advantages of this process in context of low-processing temperature, pressure-assisted sintering (pressures in the order of 40 MPa [32]) requires special tooling to avoid die fracturing at the elevated temperatures. On the other hand, at such pressures a slight irregularities can lead to cracking of brittle ceramic substrates [33]. Limitations in shape-complexity of the product and development of residual stresses are also presented.

In the present work, a novel procedure was utilized for active brazing of YSZ to SS by using nanopastes without applying a high pressure upon sintering. Silver and nickel nanoparticles with an average size of  $\sim 80$  nm were homogeneously distributed into an organic matrix, which operated as a stabilizer, binder and dispersant. The organic phase provides initial adhesion and wetting for the connection and prevents condensation of nanoparticles before brazing [34]. Here, it is noteworthy that nanopastes have recently found remarkable applications in electronic circuits, color filters, thin film transistors (TFT) for liquid crystal displays (LCD), low-temperature lead-free electronics, and flexible joints [35]. Recent studies [36] have shown that sintering of nanoparticles can be performed at relatively low temperatures due to enhanced sintering driving forces caused by high surface curvatures. Bai [37] showed that a nanopaste containing 78 vol% Ag nanoparticles with an average size of 30 nm could be sintered at 280 °C under standard atmospheric pressure to obtain fractional density of 80% theoretical with an elastic modulus of 10 GPa and tensile strength of 43 MPa. Wang et al. [38] reported shear strength of 15–20 MPa for a sintered silver nanopaste at a temperature range of 270–325 °C. We have developed silver and nickel nanopastes for brazing of YSZ to SS at relatively low temperatures of 270–360 °C. It is shown that

YSZ/SS joints can successfully be prepared without applying pressure to obtain sound interfaces with fractional density of about 80% theoretically. The microstructural features and mechanical strength of the joints are presented and the effects of processing parameters are discussed.

## 2. Experiments procedure

Bulk 5 mol% Y–ZrO<sub>2</sub> plates with a thickness of 3 mm and density of 2.7 g/cm<sup>3</sup> were supplied by Khorasan Science and Technology Park, Mashhad, Iran. Small specimens with dimensions of 18 mm × 18 mm were prepared by diamond cutting disc and diamond grinding wheel. AISI 420 stainless steel plates were prepared by a magnetic grinding machine. The joining surfaces were polished by using abrasive papers followed by mechanical polishing using 1 μm alumina (for SS) and diamond (for YSZ) pastes. Finally, the surfaces were thoroughly cleaned by ethanol washing.

Colloidal suspensions of silver and nickel nanoparticles were provided by Avijeh Company, Tehran, Iran. The nanoparticles were prepared by Electrical Explosion of Wire [39]. The concentration of silver and nickel particles in the suspension was 1 and 0.8 wt%, respectively. The average size of particles was about 80 nm having a narrow size distribution (Fig. 1a and b) with a purity of > 99%. Carboxymethyl cellulose (CMC) was supplied by SINOCMC CO. (Germany) and used as the organic phase composition of the nanopastes. It was reported that carboxymethyl and hydroxyl can provide hydrogen bonding, forming a large molecular network that can capture individual nanoparticles [40]; hence, stable nanopastes could be attained. Various amounts of CMC were added to the nanoparticle colloids to prepare nanopastes with different compositions and solid loadings (see Table 1). The mixtures were homogenized by mechanical stirring followed by ultrasonic agitation at room temperature. The process was continued until the mixtures were semi-dried and paintable pastes were obtained.

For brazing, the nanopastes were placed on the metal surfaces by using a clean needle attached to a syringe. Assembling of the joints were performed by inserting the YSZ plates on the top of metallic plates, cleaning the extra pastes from the corners, and fixing the couples by a spring-assisted fixture. The initial applied pressure on the joint interface was calibrated to  $\sim 5$  MPa. The assembled parts were loaded into a laboratory furnace and heated at a rate of 10 °C/min to desired temperature in the range of 270–360 °C and held for different times from 60 to 150 min, as reported in Table 1. Air atmosphere was utilized to catalyze burning of the organic binder by oxygen. After brazing, the samples were cooled inside the furnace. In order to determine appropriate processing conditions with minimum experimental runs, L16 Taguchi design of experiments (DOE) [41] was employed. Table 1 shows orthogonal arrays of Taguchi DOE used in this work. Four factors (solid loadings of silver and nickel, time and temperature) at four levels were evaluated. For each condition, three samples were prepared. An electronic image of the prepared joints is shown in Fig. 1c.

The brazed specimens were cut by a diamond saw for cross-sectional microstructural studies. Scanning electron microscopy

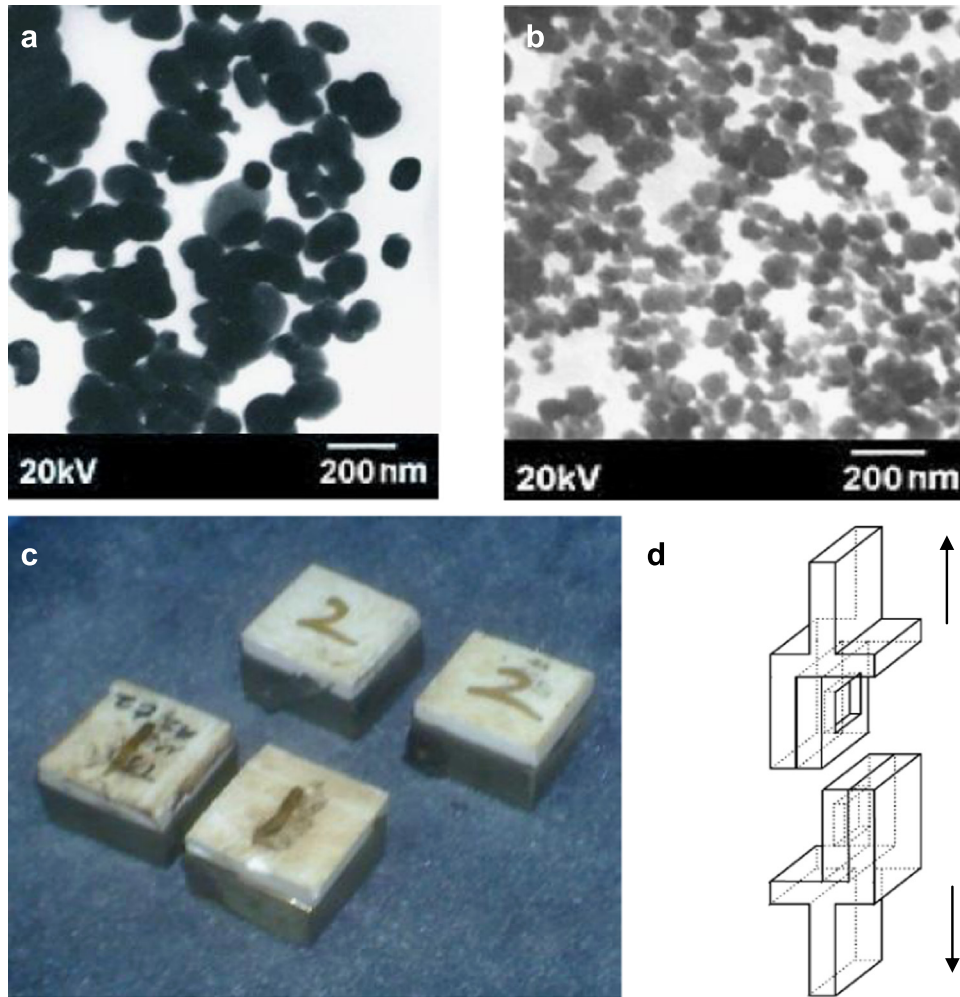


Fig. 1. TEM images show (a) silver and (b) nickel nanoparticles. (c) Digital images of YSZ-SS joints. (d) A schematic representation of the designed mold for testing of the shear strength. Arrows show the direction of applied load.

Table 1  
Chemical composition of nanopastes and the employed sintering conditions.

Sample No	Nickel (%)	Silver (%)	Solid loadings (%)	Time (min)	Temp (°C)
1	16	10	26	90	300
2	24	10	34	120	330
3	32	10	42	150	360
4	8	20	28	120	300
5	16	20	36	150	270
6	24	20	44	60	360
7	32	20	52	90	330
8	8	30	38	150	330
9	16	30	46	120	360
10	24	30	54	90	270
11	32	30	62	60	300
12	8	40	48	90	360
13	16	40	56	60	330
14	24	40	64	150	300
15	32	40	72	120	270

(SEM, JEOL, Japan) at an operating voltage of 15 kV was utilized. Electron probe micro-analyzer (EPMA, JEOL JXA-8230) was used for local chemical analysis along the interface.

The strength of the joints was determined by a shear tooling designed for this purpose (Fig. 1d). A tensile machine (Instron, UK) with a load cell of 5 kN was used. The applied strain rate was  $0.1 \text{ s}^{-1}$ .

### 3. Results and discussion

#### 3.1. Microstructure of the joint interface

Fig. 2 shows cross-sectional SEM images of a YSZ-SS couple after fracturing. This sample was prepared by employing a Ni/Ag nanopaste (No. 1 in Table 1) and sintering at  $300 \text{ }^\circ\text{C}$  for 90 min. The interface region composed of a spongy layer of sintered particles with an average thickness of  $\sim 4 \mu\text{m}$  (Fig. 2a and c). The relatively low sintering temperature did not yield full densification of the nanopaste with a high initial porosity of 76%. The sintered density of the interface region was estimated 70% of the theoretical density. Color-code EPMA images showed that the distribution of Ag and Ni in the interface region is almost uniform (Fig. 2b and d). It was also found that diffusion layer formed between the paste and SS was wider than that of YSZ/paste. The diffusion depth of

Ni in the SS part ( $\sim 1.5 \mu\text{m}$ ) was also higher than that of silver side ( $\sim 1 \mu\text{m}$ ) while both elements have a limited diffusion in the YSZ layer ( $\sim 200 \text{ nm}$ ). The higher concentration of Ni in

the nanopaste caused higher concentration gradient and thus more diffusion force to move. The higher solubility of Ni in SS and smaller atomic radius also influence the diffusion depth.

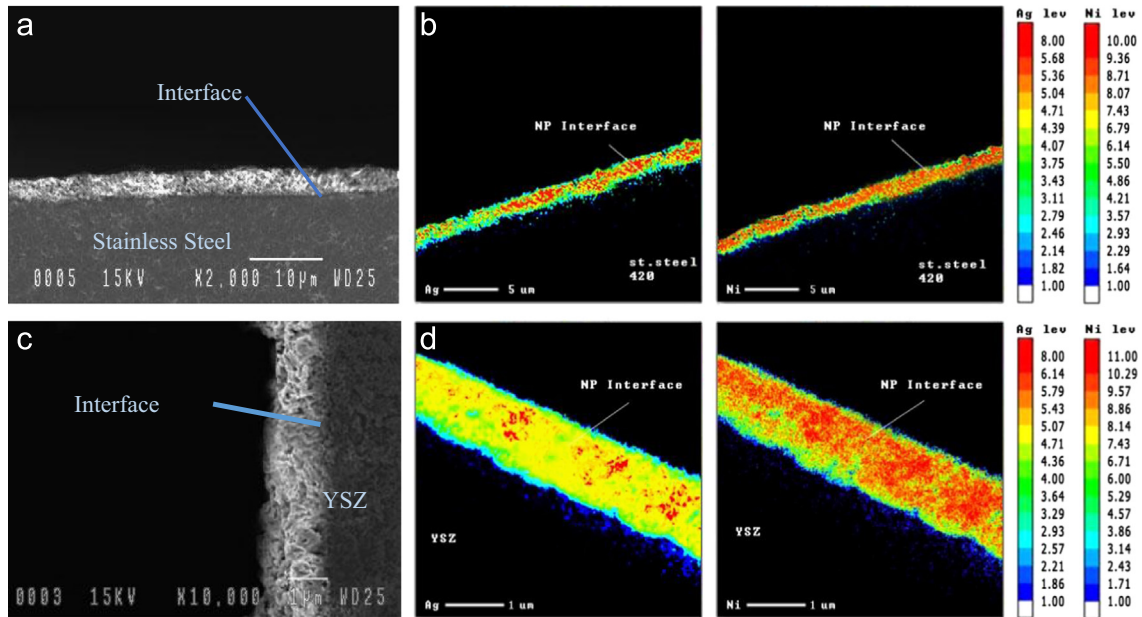


Fig. 2. Cross-sectional SEM images and EPMA analysis of a fractured joint made by pressure-less sintering of YSZ/SS couple using the nanopaste No. 1 (see Table 1).

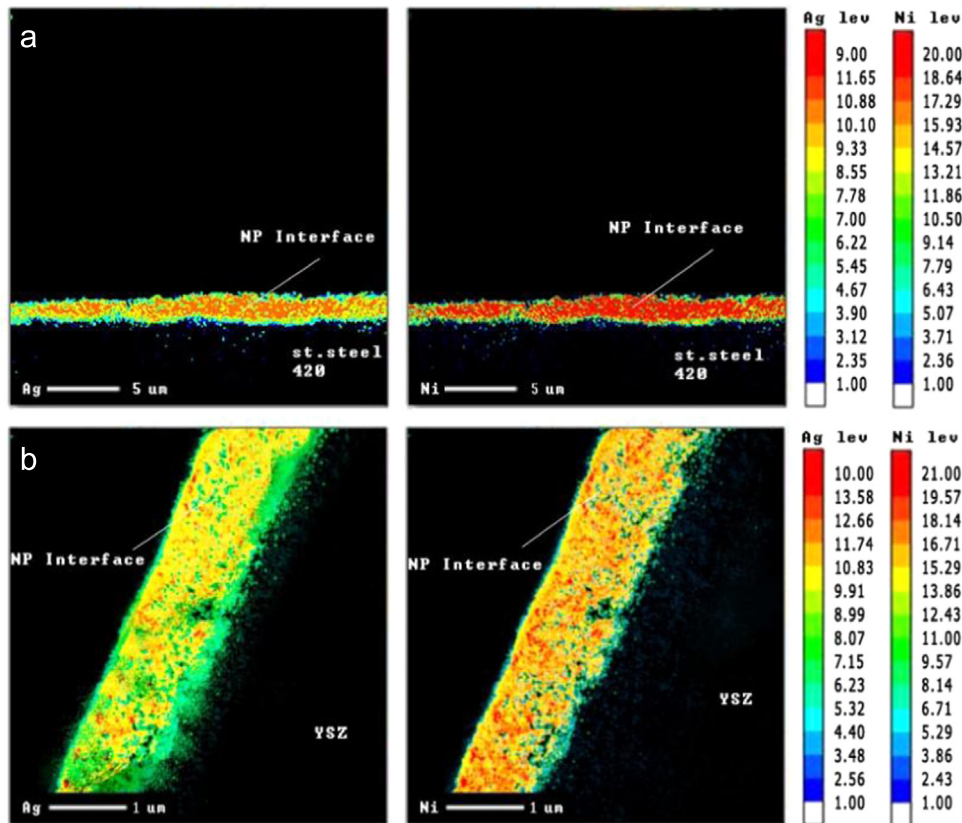


Fig. 3. EPMA analysis showing the distribution of Ag and Ni elements through the interface region of a YSZ/SS couple prepared by employing nanopaste No. 3 (see Table 1).

When a higher sintering temperature of 360 °C was utilized (No. 3 in Table 1), denser interface layer was attained (Fig. 3) due to higher sintering activity of the nanoparticles at the elevated temperature and faster diffusion rate that promotes solid-state sintering. The diffusion depths in the YSZ and SS layers were also broadened. It was also found the increasing of the solid loading and the concentration of Ag nanoparticles in the paste promoted densification during the low-temperature sintering (Fig. 4). Since the melting temperature of silver is significantly lower than Ni, increasing of Ag concentration with higher sintering activity enhanced the densification. The higher solid loading also yielded denser layer due to more initial metal–metal contacts and less initial porosity.

### 3.2. Shear strength

Table 2 reports the interface thickness, shear strength and shear modulus of YSZ–SS joints prepared at different conditions. As it was expected, the fracture occurred from the interface due to its spongy structure. In other words, the strength of this region was lower than the ceramic and metal counterparts due to the presence of pores that decreased the load-bearing area with “stress concentration effect”. The shear strength varied in the range of 14–21 MPa ( $\pm 1$  MPa) depending on the paste composition and sintering condition. It is worth noting that the range of shear strength and shear modulus obtained is in compliance with previous research [42] utilizing silver nanopastes. The results indicated the significant effect of solid loading on the joint strength. Since the shear strength of porous materials is significantly affected

by the porosity level [43], a denser interface layer exhibits higher strength. The higher Ag concentration in the nanopaste also enhanced the strength as higher density could be attained.

### 3.3. Taguchi analysis and optimization

Effects of paste composition, sintering time and temperature on the shear strength and modulus were studied. Orthogonal Taguchi design of experiments was utilized. Fig. 5 shows the results of

Table 2

Shear strength and modulus of YSZ/SS joints prepared by employing Ag/Ni nanopastes.

Sample no	Average thickness ( $\pm 0.5 \mu\text{m}$ )	Shear strength modulus (GPa $\pm 0.1$ )	Shear strength (MPa $\pm 1$ )
1	4	0.4	13.6
2	3.9	0.47	14.6
3	4.6	0.34	15/3
4	4.1	0.62	16.8
5	4.5	0.46	17.3
6	4.5	0.57	16.3
7	3.7	0.58	18.2
8	4.3	0.55	16.8
9	4.5	0.45	14.3
10	4.2	0.55	16.8
11	4.5	0.54	15.2
12	3.7	0.42	15.6
13	3.8	0.58	18.0
14	4.2	0.47	18.1
15	3.8	0.61	21.3

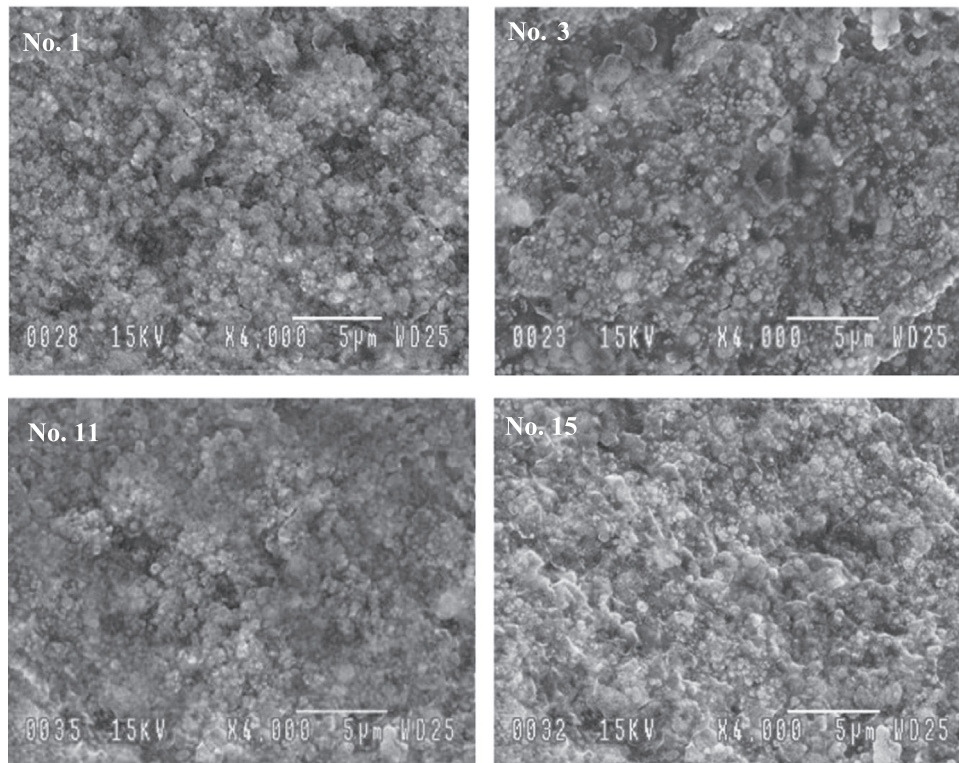


Fig. 4. SEM images showing the fracture surface of YSZ/SS couples prepared by employing Ag/Ni nanopastes. The solid loading (%) was: (a) 26, (No. 1) (b) 42 (No. 3), (c) 62 (No. 11), (d) 72 (No. 15).

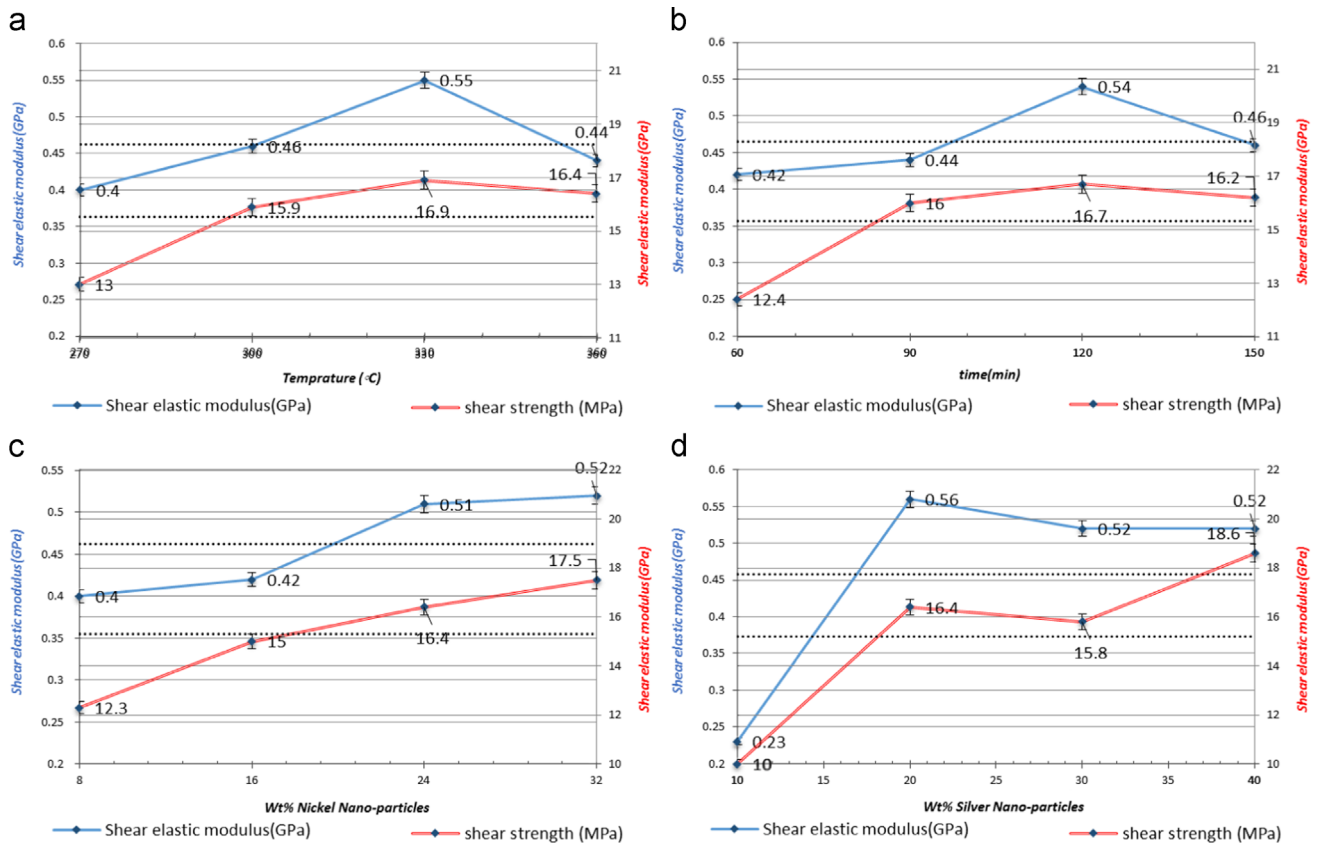


Fig. 5. ANOVA analysis of the experimental results designed by L16 Taguchi array. Average effects of each factor including (a) sintering temperature, (b) sintering time, (c) silver concentration, and (d) nickel concentration on the shear strength and modulus are illustrated. The solid lines only show the trend of variations.

DOE analysis. The effect of sintering temperature is shown in Fig. 5a. As seen, increasing the temperature up to 330 °C improved the strength and modulus. The higher sintering promotes densification and thus more load-bearing of the interface layer. However, sintering at 360 °C slightly decreased the strength. The effect of sintering time is shown in Fig. 5b. It was found the prolonged sintering time at a constant temperature had a marginal effect on the strength and modulus. By increasing the concentration of silver and/or nickel nanoparticles, a higher shear strength/modulus was obtained (Fig. 5c and d). Meanwhile, the effect of Ag concentration was more pronounced than the Ni content do. In order to determine the most significant factors affecting the strength of the joints, ANOVA analysis was performed. While it was possible to determine the interactions between different parameters, the contribution of each factor on the shear strength and shear elastic modulus was examined by [41]:

$$P_A = \frac{S_A}{S_T} \times 100 = \frac{\left( \sum_{i=1}^z A_i^2 / N_{A_i} \right) - \left( \left( \sum_{i=1}^n y_i^2 \right) / n \right)}{\left( \sum_{i=1}^n y_i^2 \right) - \left( \left( \sum_{i=1}^n y_i^2 \right) / n \right)} \times 100 \quad (1)$$

where  $P_A$  is the contribution of factor A,  $S_T$  is total sum of squares,  $S_A$  is sum of the squares of the A factor, and  $n$  is the number of experiments. For the  $i$ th level,  $A_i$  is the test output (result) and  $N_{A_i}$  is number of tests.  $y_j$  is the result in  $i$ th level of the experiments. Fig. 6 shows the results of ANOVA analysis to indicate the

contribution of each factor. It was found that the silver solid loading has the vital role on the strength followed by Ni concentration. The effect of solid layer loading can be explained by higher density of the interface layer but the effect of Ni is inter-diffusion of Ni in the couple to prepare stronger contact. The effect of temperature was also more pronounced than time. ANOVA analysis showed that the most proper condition for joining could be attained by a nanopaste with 72% solid loading sintered at 330 °C for 120 min. Under this circumstance, the predicated shear strength would be  $23.3 \pm 1$  MPa. The predicated value is close to the measured value of  $21 \pm 1$  MPa for the YSZ/SS joint sintered at slightly lower temperature (270 °C). This means that employing higher sintering temperatures is useful to enhance densification of the bonding layer in order to attain a higher joint strength.

#### 4. Conclusions

Pressure-less joining of 5Y-stabilized zirconia to 420 AISI SS at low temperatures (< 370 °C) was studied. The main findings can be summarized as follows:

- A mixture of silver and nickel nanoparticles can be used to prepare nanopastes for sound joining of YSZ to SS.
- Pressure-less sintering of YSZ–SS couples at low temperatures yielded a porous interface layer. The density of the

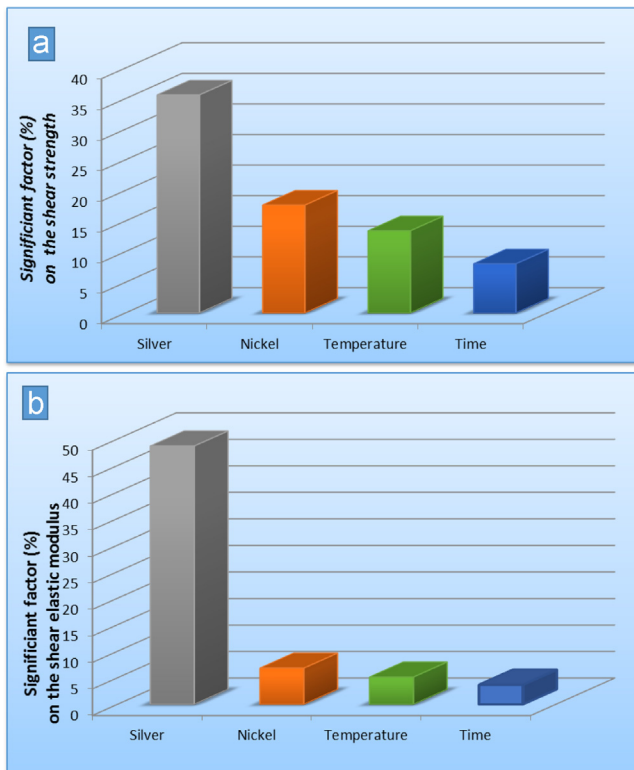


Fig. 6. ANOVA analysis presents the contribution of each factor on the (a) shear strength and (b) shear modulus of YSZ/SS joints.

interface region depended on the amount of solid loading, the composition of the paste, and sintering condition.

- Limited diffusion of the paste elements in the joint counterparts was noticed. The diffusion depth of Ni was more than that of Ag diffusion.
- DOE analysis showed that solid loading of the nanopaste has the most important factor affecting the strength of the joints followed by the concentration of nickel.
- The highest shear strength was attained for a 32/40 Ag/Ni paste with 72% solid loading.

## References

- [1] Y. Liang, S.P. Dutta, Application trend in advanced ceramic technologies, *Technovation* 21 (2001) 61–65, [http://dx.doi.org/10.1016/S0166-4972\(00\)00019-5](http://dx.doi.org/10.1016/S0166-4972(00)00019-5).
- [2] F. Tietz, P. Nikolopoulos, Metal/ceramic interface properties and their effects on sofc development, *Fuel Cells* (2009) 867–872, <http://dx.doi.org/10.1002/fuce.200800125>.
- [3] T. Tanaka, K. Matsumura, H. Komorita, N. Mizunoya, Bonded ceramic metal composite substrate, circuit board constructed therewith and methods for production thereof, *Microelectron. Reliab.* 31 (1991) 1058, [http://dx.doi.org/10.1016/0026-2714\(91\)90192-A](http://dx.doi.org/10.1016/0026-2714(91)90192-A).
- [4] R. Nagel, H. Hahn, A. Balogh, Diffusion processes in metal/ceramic interfaces under heavy ion irradiation, *Nucl. Instrum. Method. Phys. Res. Sect. B Beam Interact. Mater. Atoms.* 148 (1999) 930–935 [http://dx.doi.org/10.1016/S0168-583X\(98\)00883-0](http://dx.doi.org/10.1016/S0168-583X(98)00883-0).
- [5] S. Affatato, M. Spinelli, S. Squarzone, F. Traina, A. Toni, Mixing and matching in ceramic-on-metal hip arthroplasty: an in-vitro hip simulator study, *J. Biomech.* 42 (2009) 2439–2446, <http://dx.doi.org/10.1016/j.jbiomech.2009.07.031>.
- [6] A.K. Ray, S.C. Bose, P.K. De, D.K. Das, Lifetime evaluation of a thick thermal barrier coated superalloy used in turbine blade, *Mater. Sci. Eng. A* 527 (2010) 5474–5483, <http://dx.doi.org/10.1016/j.msea.2010.06.005>.
- [7] Z. Yong, F. Di, Progress in joining ceramics to metals, *J. Iron Steel Res., Int.* 13 (2006) 01–05.
- [8] R.M. Do Nascimento, A.E. Martinelli, A.J.A. Buschineli, Review article: recent advances in metal-ceramic brazing, *Ceramica* 49 (2003) 178–198.
- [9] I. Nikellis, A. Levi, S. Zinelis, Effect of soldering on the metal-ceramic bond strength of an Ni–Cr base alloy, *J. Prosthet. Dent.* 94 (2005) 435–439, <http://dx.doi.org/10.1016/j.prosdent.2005.09.012>.
- [10] E. Tamjid, A. Simchi, T. Hartwig, Co-sintering of nanoscaled zirconia powder to stainless steels for manufacturing functionally graded composite layers, in: Proceedings of the 1st International Congress on Nanoscience & Nanotechnology, Iranian Nanotechnology Society, Tehran, 2006.
- [11] C. Shearwood, Y.Q. Fu, L. Yu, K.A. Khor, Spark plasma sintering of TiNi nano-powder, *Scr. Mater.* 52 (2005) 455–460, <http://dx.doi.org/10.1016/j.scriptamat.2004.11.010>.
- [12] M. Birkholz, U. Albers, T. Jung, Nanocomposite layers of ceramic oxides and metals prepared by reactive gas-flow sputtering, *Surf. Coatings Technol.* 179 (2004) 279–285, [http://dx.doi.org/10.1016/S0257-8972\(03\)00865-X](http://dx.doi.org/10.1016/S0257-8972(03)00865-X).
- [13] J.Q. Li, X.R. Zeng, J.N. Tang, P. Xiao, Fabrication and thermal properties of a YSZ–NiCr joint with an interlayer of YSZ–NiCr functionally graded material, *J. Eur. Ceram. Soc.* 23 (2003) 1847–1853.
- [14] F. Smeacetto, M. Salvo, M. Ferraris, V. Casalegno, P. Asinari, A. Chrysanthou, Characterization and performance of glass–ceramic sealant to join metallic interconnects to YSZ and anode-supported-electrolyte in planar SOFCs, *J. Eur. Ceram. Soc.* 28 (2008) 2521–2527, <http://dx.doi.org/10.1016/j.jeurceramsoc.2008.03.035>.
- [15] E.P. Busso, Z.Q. Qian, A mechanistic study of microcracking in transversely isotropic ceramic-metal systems, *Acta Mater.* 54 (2006) 325–338, <http://dx.doi.org/10.1016/j.actamat.2005.09.003>.
- [16] K.A.U. Khor, Y.W. Gu, Thermal properties of plasma-sprayed functionally graded thermal barrier coatings, *Thin Sol. Films* (2000) 104–113.
- [17] Y. Bai, Z.H. Han, Surface & coatings technology structure–property differences between supersonic and conventional atmospheric plasma sprayed zirconia thermal barrier coatings, *Surf. Coat. Technol.* 205 (2011) 3833–3839, <http://dx.doi.org/10.1016/j.surfcoat.2011.01.056>.
- [18] M. Ferraris, E. Verne, P. Appendino, C. Moisesescu, A. Krajewski, A. Ravaglioli, et al., Coatings on zirconia for medical applications, *J. Mater. Sci.* 21 (2000) 765–773.
- [19] L. Amelinckx, M. Kamrunnahar, P. Chou, D.D. Macdonald, Figure of merit for the quality of ZrO<sub>2</sub> coatings on stainless steel and nickel-based alloy surfaces, *Corros. Sci.* 48 (2006) 3646–3667, <http://dx.doi.org/10.1016/j.corsci.2005.12.005>.
- [20] D.T. Llewellyn, R.C. Hudd, *Steels*, Elsevier <http://dx.doi.org/10.1016/B978-075063757-2/50004-4>.
- [21] Q.-L. Xiao, C. Xu, S.-Y. Shao, J.-D. Shao, Z.-X. Fan, Y<sub>2</sub>O<sub>3</sub> stabilized ZrO<sub>2</sub> thin films deposited by electron-beam evaporation: optical properties, structure and residual stresses, *Vacuum* 83 (2008) 366–371 <http://dx.doi.org/10.1016/j.vacuum.2008.05.031>.
- [22] Z.E. Sánchez-Hernández, M.A. Domínguez-Crespo, A.M. Torres-Huerta, E. Onofre-Bustamante, J. Andraca Adame, H. Dorantes-Rosales, Improvement of adhesion and barrier properties of biomedical stainless steel by deposition of YSZ coatings using RF magnetron sputtering, *Mater. Charact.* 91 (2014) 50–57, <http://dx.doi.org/10.1016/j.matchar.2014.02.007>.
- [23] B. Ferrari, I.M. de Francisco, R. Moreno, Ni–YSZ self-supported films by gel electrophoresis, *Ceram. Int.* 31 (2005) 863–868, <http://dx.doi.org/10.1016/j.ceramint.2004.09.014>.
- [24] H. Tikkanen, C. Suci, I. Wærnhus, A.C. Hoffmann, Examination of the co-sintering process of thin 8YSZ films obtained by dip-coating on in-house produced NiO–YSZ, *J. Eur. Ceram. Soc.* 31 (2011) 1733–1739 <http://dx.doi.org/10.1016/j.jeurceramsoc.2011.03.015>.

- [25] P. Stefanov, D. Stoychev, I. Valov, A. Kakanakova-georgieva, T. Marinova, Electrochemical deposition of thin zirconia films on stainless steel 316 L, *Mater. Chem. Phys.* 65 (2000) 222–225.
- [26] E. Jime, E. Lara-curzio, M. Singh, Microstructure and mechanical properties of superplastically joined yttria-partially-stabilized zirconia ( Y-PSZ ) ceramics, *J. Eur. Ceram. Soc.* 20 (2000) 147–151.
- [27] W.B. Hanson, K.I. Ironside, J.A. Fernie, Active metal brazing of zirconia, *Acta Metall.* 48 (2000) 4673–4676.
- [28] M. Singh, T.P. Shpargel, Brazing of yttria-stabilized zirconia (YSZ ) to stainless steel using Cu, Ag, and Ti-based brazes, *J. Mater. Sci.* 43 (2008) 23–32, <http://dx.doi.org/10.1007/s10853-007-1985-z>.
- [29] M. Singh, T.P. Shpargel, R. Asthana, Braze oxidation behavior and joint microstructure in YSZ/steel joints made using palladium brazes for SOFC applications, *Mater. Sci. Eng. A* 485 (1-2) (2008) 670–695, <http://dx.doi.org/10.1016/j.msea.2007.08.032>.
- [30] P. Ried, C. Lorenz, A. Brönstrup, T. Graule, N.H. Menzler, W. Sitte, et al., Processing of YSZ screen printing pastes and the characterization of the electrolyte layers for anode supported SOFC, *J. Eur. Ceram. Soc.* 28 (2008) 1801–1808, <http://dx.doi.org/10.1016/j.jeurceramsoc.2007.11.018>.
- [31] C. Herring, Effect of change of scale on sintering phenomena, *J. Appl. Phys.* 2 (4) (1950) 301–303, <http://dx.doi.org/10.1007/s11664-007-0230-5>.
- [32] I. De Microelectrónica, D.B.N. De Microelectronica, Silver nano-particles sintering process for the die-attach of power devices for high temperature applications, *Ing. Mec.* 4 (2012) 97–102.
- [33] Y. Mei, G. Chen, G. Lu, X. Chen, Effect of joint sizes of low-temperature sintered nano-silver on thermal residual curvature of sandwiched assembly, *Int. J. Adhes. Adhes.* 35 (2012) 88–93, <http://dx.doi.org/10.1016/j.ijadhadh.2011.12.010>.
- [34] S.B. Rane, T. Seth, G.J. Phatak, D.P. Amalnerkar, B.K. Das, Influence of surfactants treatment on silver powder and its thick films, *Mater. Lett.* 57 (2003) 3096–3100, [http://dx.doi.org/10.1016/S0167-577X\(03\)00003-X](http://dx.doi.org/10.1016/S0167-577X(03)00003-X).
- [35] P. Peng, A. Hu, B. Zhao, Reinforcement of Ag nanoparticle paste with nanowires for low temperature pressureless bonding, *J. Mater. Sci.* 47 (2012) 6801–6811, <http://dx.doi.org/10.1007/s10853-012-6624-7>.
- [36] K.S. Siow, Review: mechanical properties of nano-silver joints as die attach materials, *J. Alloys Compd.* 514 (2012) 6–19, <http://dx.doi.org/10.1016/j.jallcom.2011.10.092>.
- [37] G. Bai, Low-Temperature Sintering of Nanoscale Silver Paste for Semiconductor Device Interconnection, Virginia Polytechnic Institute and State University, 2005.
- [38] T. Wang, X. Chen, G.-Q. Lu, G.-Y. Lei, Low-temperature sintering with nano-silver paste in die-attached interconnection, *J. Electron. Mater.* 36 (2007) 1333–1340, <http://dx.doi.org/10.1007/s11664-007-0230-5>.
- [39] G. Skandon, Processing of nanostructured zirconia ceramics, *Nanostruct. Mater.* 5 (February (2)) (1995) 111–126.
- [40] A.C. Hoeffler, Sodium Carboxymethyl Cellulose Chemistry, Functionality, And Applications, Food Ingredients Group, Hercules Incorporated, Wilmington, Delaware, 2003, p. 1–15.
- [41] P.J. Ross Taguchi, *Techniques for Quality Engineering*, 2nd edition, McGraw-Hill Book Co., New York, 1996.
- [42] T. Wang, G. Chen, Y. Wang, X. Chen, G. Lu, Uniaxial ratcheting and fatigue behaviors of low-temperature sintered nano-scale silver paste at room and high temperatures, *Mater. Sci. Eng. A* 527 (2010) 6714–6722, <http://dx.doi.org/10.1016/j.msea.2010.07.012>.
- [43] J. Hadizadeh, R. Sehhati, T. Tullis, Porosity and particle shape changes leading to shear localization in small-displacement faults, *J. Struct. Geol.* 32 (2010) 1712–1720, <http://dx.doi.org/10.1016/j.jsg.2010.09.010>.